Reduced Anionic Mn_{12} Molecules with Half-Integer Ground States as Single-Molecule Magnets

Sheila M. J. Aubin,[†] Ziming Sun,[†] Luca Pardi,[‡] J. Krzystek,[‡] Kirsten Folting,[§] Louis-Claude Brunel,[‡] Arnold L. Rheingold,[||] George Christou,*[,§] and David N. Hendrickson*[,†]

Department of Chemistry and Biochemistry-0358, University of California at San Diego, La Jolla, California 92093-0358, Center for Interdisciplinary Magnetic Resonance, National High Magnetic Field Laboratory, Florida State University, Tallahassee, Florida 32310, Department of Chemistry, University of Delaware, Newark, Delaware 19716, and Department of Chemistry, and Molecular Structure Center, Indiana University, Bloomington, Indiana, 47405

Received May 25, 1999

The preparation, characterization, and X-ray structure are reported for the single-molecule magnet $(PPh_4)[Mn_{12}O_{12}(O_2CPh)_{16}(H_2O)_4]\cdot 8(CH_2Cl_2)$ (**2**). Complex **2** crystallizes in the triclinic space group $P\bar{1}$, which at 213 K has $a = 17.2329(2)$, $b = 17.8347(2)$, $c = 26.8052(2)$ Å, $\alpha = 90.515(2)$, $\beta = 94.242(2)$, $\gamma = 101.437(2)°$, and $Z = 2$. The salt consists of PPh_4^+ cations and $[Mn_{12}O_{12}(O_2CPh)_{16}(H_2O)_4]^-$ anions. The $(Mn_{12}O_{12})^{15+}$ core of the anion is formed by an external ring of eight Mn atoms bridged by μ_3−O^{2-} ions to an internal tetrahedron of four Mn atoms. Because of disorder in both phenyl rings and solvate molecules, it was difficult to use bond valence sum values to determine definitively the oxidation state of each Mn atom. There is a Mn_4O_4 cubane unit in the internal part of the molecule and these Mn atoms are all Mn^{IV} ions. For the eight "external" Mn atoms the bond valence sum values did *not* define well their oxidation states. For these eight Mn atoms, it was not possible to determine whether a trapped-valence $Mn^{II}Mn^{III}_7$ or an electronically delocalized description is appropriate. High-frequency EPR (HFEPR) data were collected for the previously structurally characterized $Mn^{IV}_4Mn^{III}_7Mn^{II}$ valence-trapped salt $(PPh_4)[Mn_{12}O_{12}(O_2CEt)_{16}(H_2O)_4]$ (**1**) at 328.2 and 437.69 GHz. In the high magnetic field the crystallites orient and the HFEPR spectra are pseudo−single-crystal like, not powder patterns. The spectral features are attributed to the fine structure expected for a $S = 19/2$ complex experiencing axial zero-field splitting $D\hat{S}_z^2$, where $D = -0.62$ cm^{-1}. The sign of D was definitively determined by the temperature dependence of the spectrum. Complex **2** exhibits one out-of-phase ac magnetic susceptibility (χ''_M) signal in the 3−6 K range. The temperature of the χ''_M peak is frequency dependent, as expected for a single-molecule magnet. The rate at which the direction of magnetization reverses from "up" to "down" was evaluated from χ''_M data collected at various frequencies (1−1512 Hz) of oscillation of the ac magnetic field. This gives magnetization relaxation rates in the 2.86−4.51 K range for complex **2** and in the 3.2−7.2 K range for complex **1**. Rates were also determined in the 1.80−2.50 K range for complex **1** via magnetization decay experiments. In this latter case, the polycrystalline sample is magnetically saturated in a large dc field. After the magnetic field is rapidly decreased to zero, the decay of the magnetization to zero is monitored. The rates evaluated by both the frequency dependence of the out-of-phase ac signal and dc relaxation decay experiments for complex **1** fit on an Arrhenius plot to give an activation energy of $U_{eff} = 57$ K and a preexponential rate of $1/\tau_0 = 7.2 \times 10^7$ s^{-1}. From the HFEPR data, complex **1** has a $S = 19/2$ ground state with $D = -0.62$ cm^{-1}. This gives a potential-energy barrier of $U = 79$ K for the double-well potential-energy diagram. The value of U_{eff} is less than the barrier height U, because when individual $[Mn_{12}^-]$ anions convert from spin "up" to spin "down", they can not only be thermally activated to go over the $U = 79$ K barrier, they can also quantum mechanically tunnel through the barrier between $m_s = -n$ and $m_s = n$ levels. A multiphonon Orbach process involving molecules absorbing phonon energies and being excited incrementally from one m_s level to another is likely involved at these low temperatures below 10 K.

Introduction

The miniaturization of information storage devices drives the search for new magnetic materials. Single-molecule magnets (SMMs) are considered as candidates for high-density memory devices because: (i) each molecule is on the order of 10−20 Å in diameter and therefore could potentially be used in storing a large density of information[1]; (ii) single-molecule magnets could also be used in quantum computers[2]; and (iii) from a fundamental point of view, understanding the magnetic properties of these molecules is important because it will help to bridge the gap between the quantum and classical understanding of magnetism.[3]

[†] University of California at San Diego.
[‡] Florida State University.
[§] Indiana University.
[||] University of Delaware.

(1) Dahlberg, E. D.; Zhu, J.-G *Phys. Today* **1995**, 34.
(2) (a) Berman, G. P.; Doolen, G. D.; Holm, D. D.; Tsifrinovich, V. I. *Phys. Lett. A* **1994**, *193*, 444. (b) Garanin, D. A.; Chudnovsky, E. M. *Phys. Rev. B.* **1997**, *56*, 11102.

10.1021/ic990613g CCC: $18.00
Published on Web 10/26/1999

For SMMs, each molecule functions as a superparamagnet. The source of the magnetic anisotropy is the molecule's high-spin ground state combined with appreciable zero-field splitting. The magnetic moment of a molecule has two preferred orientations, "up" or "down" relative to the molecule's axial anisotropy axis (i.e., *z*-axis). At certain temperatures, when the thermal energy is much smaller than the energy of the barrier to flip the spin from "up" to "down", the magnetic moment of the molecule is only able to sluggishly convert from up to down. Slow magnetization relaxation is evident, leading to unusual magnetic properties: (i) steps in the magnetization hysteresis loop; (ii) frequency-dependent out-of-phase ac magnetic susceptibility signals; (iii) a divergence between the zero-field−cooled and field−cooled magnetization at the "blocking" temperature; and (iv) slow magnetization decay behavior after an external field is removed when the temperature is below the "blocking temperature." Magnetization hysteresis loops and out-of-phase ac susceptibility signals are seen for frozen solutions of SMMs or for polymer-doped samples, which indicates that these properties are caused by individual molecules[4−7] and not by long-range ordering as is commonly observed in superparamagnetic single-domain particles of a metal oxide. The fact that the slow magnetization phenomena are caused by individual molecules also is strongly supported by the lack of any anomaly in adiabatic heat-capacity measurements collected in zero field on polycrystalline samples of these SMMs.[8,9] If the sluggish magnetization relaxation was due to magnetic exchange interactions between molecules, then there would be a magnetic ordering temperature, and a thermal effect would be seen at the ordering (blocking) temperature.

The SMM field is now established and a few families of molecules are currently known to function as SMMs. The first and the most thoroughly studied SMM is $[Mn_{12}O_{12}(O_2CCH_3)_{16}(H_2O)_4]\cdot 4H_2O\cdot 2HO_2CCH_3$,[45,9−53] commonly called "$Mn_{12}Ac$" or even simply "Mn_{12}". In this family, several other structurally related dodecanuclear manganese complexes have been characterized such as $[Mn_{12}O_{12}(O_2CR)_{16}(H_2O)_x]$ [R = Et,[54−56] where $x = 3$; R = Ph,[57,58] where $x = 4$; R = Ph-2-X (X is either Cl or Br),[59] and $x = 4$; and R = Ph-4-Me, two crystal forms,[7,60] where $x = 4$]. A second family of Mn complexes

(3) (a) Awschalom, D. D.; Di Vincenzo, D. P. *Phys. Today* **1995**, *48*, 43. (b) Leslie-Pelecky, D. L.; Rieke, R. D. *Chem. Mater.* ***1996***, *8*, 1770. (c) Gunther, L. *Phys. World* **1990**, December, 28. (d) Awschalom, D. D.; Di Vincenzo, D. P.; Smyth, J. F. *Science* **1992**, *258*, 414. (e) Stamp, P. C. E.; Chudnosvsky, E. M.; Barbara, B. *Int. J. Mod. Phys.* **1992**, *B6*, 1355. (f) Gider, S.; Awschalom, D. D.; Douglas, T.; Mann, S.; Chaparala, M. *Science* **1995**, *268*, 77. (g) Politi, R.; Rettori, A.; Hartmann-Boutron, F.; Villain, J. *Phys. Rev. Lett*. **1995**, *75*, 537.

(4) (a) Sessoli, R. *Mol. Cryst. Liq. Cryst.* **1995**, *274*, 145. (b) Caneschi, A.; Gatteschi, D.; Sessoli, R.; Novak, M. A. *Nature* **1993**, *365*, 141.

(5) Eppley, H. J.; Tsai, H.-L.; de Vries, N.; Folting, K.; Christou, G.; Hendrickson, D. N. *J. Am. Chem. Soc*. **1995**, *117*, 301.

(6) Aubin, S. M. J.; Wemple, M. W.; Adams, D. M.; Tsai, H.-L.; Christou, G.; Hendrickson, D. N. *J. Am. Chem. Soc*. **1996**, *I118*, 7746.

(7) Aubin, S. M. J.; Eppley, H. J.; Guzei, I. A.; Folting, K.; Gantzel, P. K.; Rheingold, A. L.; Christou, G.; Hendrickson, D. N., manuscript submitted for publication.

(8) Sorai, M.; Eppley, H. J.; Aubin, S. M. J.; Christou, G.; Hendrickson, D. N., unpublished results.

(9) Novak, M. A.; Sessoli, R.; Caneschi, A.; Gatteschi, D. *J. Magn. Magn. Mater*. **1995**, *146*, 211.

(10) Lis, T. *Acta Crystallogr*. **1980**, *B36*, 2042.

(11) Caneschi, A.; Gatteschi, D.; Sessoli, R.; Barra, A. L.; Brunel, L. C.; Guillot, M. *J. Am. Chem. Soc*. **1991**, *113*, 5873.

(12) Sessoli, R.; Gatteschi, D.; Caneschi, A.; Novak, M. A. *Nature* **1993**, *365*, 141.

(13) Gatteschi, D.; Caneschi, A.; Pardi, L.; Sessoli, R. *Science* **1994**, *265*, 1054.

(14) Boyd, P. D. W.; Li, Q.; Vincent, J. B.; Folting, K.; Chang, H.-R.; Streib, W. E.; Huffman, J. C.; Christou, G.; Hendrickson, D. N. *J. Am. Chem. Soc*. **1988**, *110*, 8537.

(15) Villain, J.; Hartmann-Boutron, F.; Sessoli, R.; Rettori, A. *Europhys. Lett*. **1994**, *27*, 159.

(16) Barra, A. L.; Caneschi, A.; Gatteschi, D.; Sessoli, R. *J. Am. Chem. Soc*. **1995**, *117*, 885.

(17) Novak, M. A.; Sessoli, R.; Caneschi, A.; Gatteschi, D. *J. Magn. Magn. Mater*. **1995**, *146*, 211.

(18) Barbara, B.; Wernsdorfer, W.; Sampaio, L. C.; Park, J. G.; Paulsen, C.; Novak, M. A.; Ferré, R.; Mailly, D.; Sessoli, R.; Caneschi, A.; Hasselbach, K.; Benoit, A.; Thomas, L. *J. Magn. Magn. Mater*. **1995**, *140*−*144*, 1825.

(19) Novak, M. A.; Sessoli, R. In *Quantum Tunneling of Magnetization-QTM′94*; Gunther, L., Barbara, B., Eds.; Kluwer Academic Publishers: Dordrecht, 1995; pp 171−188.

(20) Paulsen, C.; Park, J.-G. In *Quantum Tunneling of Magnetization-QTM′94*; Gunther, L., Barbara, B., Eds; Kluwer Academic Publishers: Dordrecht, 1995; pp 189−207.

(21) Paulsen, C.; Park, J.-G.; Barbara, B.; Sessoli, R.; Caneschi, A. *J. Magn. Magn. Mater*. **1995**, *140*−*144*, 379.

(22) Paulsen, C.; Park, J. G.; Barbara, B.; Sessoli, R.; Caneschi, A. *J. Magn. Magn. Mater*. **1995**, *140*−*144*, 1891.

(23) Politi, R.; Rettori, A.; Hartmann-Boutron, F.; Villain, J. *Phys. Rev. Lett*. **1995**, *75*, 537.

(24) Friedman, J. R.; Sarachik, M. P.; Tejada, J.; Maciejewski, J.; Ziolo, R. *J. Appl. Phys*. **1996**, *79*, 6031.

(25) (a) Friedman, J. R.; Sarachik, M. P.; Tejada, J.; Ziolo, R. *Phys. Rev. Lett*. **1996**, *76*, 3830. (b) Friedman, J. R. Ph.D. Thesis, The City College of New York, New York City, NY, 1996.

(26) Thomas, L.; Lionti, F.; Ballou, R.; Gatteschi, D.; Sessoli, R.; Barbara, B. *Nature* **1996**, *383*, 145.

(27) Tejada, J.; Ziolo, R. F.; Zhang, X. X. *Chem. Mater*. **1996**, *8*, 1784.

(28) Hernandez, J. M.; Zhang, X. X.; Luis, F.; Bartolomé, J.; Tejada, J.; Ziolo, R. *Europhys. Lett*. **1996**, *35*, 301.

(29) Chudnovsky, E. M. *Science* **1996**, *274*, 938.

(30) Reynolds, P. A.; Gilvert, E. P.; Figgis, B. N. *Inorg. Chem*. **1996**, *35*, 545.

(31) Gatteschi, D. *Curr. Opin. Solid State Mater. Sci*. **1996**, *1*, 192.

(32) Burin, A. L.; Prokof′ev, N. V.; Stamp, P. C. E. *Phys. Rev. Lett*. **1996**, *76*, 3040.

(33) Politi, P.; Rettori, A.; Hartmann-Boutron, F.; Villain, J. *Phys. Rev. Lett*. **1996**, *76*, 3041.

(34) Schwarzschild, B. *Phys. Today* **1997**, January 17.

(35) Lionti, F.; Thomas, L.; Ballou, R.; Barbara, B.; Sulpice, A.; Sessoli, R.; Gatteschi, D. *J. Appl. Phys*. **1997**, *81*, 4608.

(36) Friedman, J. R.; Sarachik, M. P.; Hernandez, J. M.; Zhang, X. X.; Tejada, J.; Molins, E.; Ziolo, R. *J. Appl. Phys.* ***1997***, *81*, 3978.

(37) Barra, A. L.; Gatteschi, D.; Sessoli, R. *Phys. Rev. B* **1997**, *56*, 8192.

(38) Luis, F.; Bartolomé, J.; Fernández, J. F. *Phys. Rev. B* **1997**, *55*, 11448.

(39) Hernandez, J. M.; Zhang, X. X.; Luis, F.; Tejada, J.; Friedman, J. R.; Sarachik, M. P.; Ziolo, R. *Phys. Rev. B* **1997**, *55*, 5858.

(40) Cheesman, M. R.; Oganesyan, V. S.; Sessoli, R.; Gatteschi, D.; Thomson, A. J. *Chem. Commun*. **1997**, 1677.

(41) Caneschi, A.; Gatteschi, D.; Sessoli, R. *J. Chem. Soc., Dalton Trans*. **1997**, 3963.

(42) Fort, A.; Rettori, A.; Villain, J.; Gatteschi, D.; Sessoli, R. *Phys. Rev. Lett*. **1998**, *80*, 612.

(43) Zhang, X. X.; Tejada, J.; Hernandez, J. M.; Ziolo, R. F. *NanoStruct. Mater*. **1997**, *9*, 301.

(44) Lascialfari, A.; Gatteschi, D.; Borsa, F.; Shastri, A.; Jang, Z. H.; Carretta, P. *Phys. Rev. B* **1998**, *57*, 514.

(45) Hill, S.; Perenboon, J. A. A. J.; Dalal, N. S.; Hathaway, T.; Stalcup, T.; Brooks, J. S. *Phys. Rev. Lett*. **1998**, *80*, 2453.

(46) Chudnovsky, E. M.; Garanin, D. A. *Phys. Rev. Lett*. **1997**, *79*, 4469.

(47) Garanin, D. A.; Chudnovsky, E. M. *Phys. Rev. B* **1997**, *56*, 11102.

(48) Wei, Y.-G.; Zhang, S.-W.; Shao, M.-C.; Tang, Y.-Q. *Polyhedron* **1997**, *16*, 1471.

(49) Luis, F.; Bartolomé, J.; Fernández, J. F. *Phys. Rev. B* **1998**, *57*, 505.

(50) Forminaya, F.; Villain, J.; Gandit, P.; Chaussy, J.; Caneschi, A. *Phys. Rev. Lett*. **1997**, *79*, 1126.

(51) Barra, A.-L.; Debrunner, P.; Gatteschi, D.; Schulz, Ch. E.; Sessoli, R. *Europhys. Lett*. **1996**, *35*, 133.

(52) Sangregorio, C.; Ohm, T.; Paulsen, C.; Sessoli, R.; Gatteschi, D. *Phys. Rev. Lett.* **1997**, *78*, 4645.

(53) Barra, A. L.; Gatteschi, D.; Sessoli, R. *Phys. Rev. B* **1997**, *56*, 8192.

(54) Eppley, H. J.; Wang, S.; Tsai, H.-L.; Aubin S. M.; Folting, K.; Streib, W. E.; Hendrickson, D. N.; Christou, G. *Mol. Cryst. Liq. Cryst*. **1995**, *274*, 159.

(55) Tsai, H.-L.; Eppley, H. J.; de Vries, N.; Folting, K.; Christou, G.; Hendrickson, D. N. *Mol. Cryst. Liq. Cryst*. **1995**, *274*, 167.

(56) Eppley, H. J.; Aubin, S. M. J.; Wemple, M. W.; Adams, D. M.; Tsai, H.-L.; Grillo, V. A.; Castro, S. L.; Sun, Z.; Folting, K.; Huffman, J. C.; Hendrickson, D., N.; Christou, G. *Mol. Cryst. Liq. Cryst*. **1997**, *305*, 167.

with a $[Mn^{IV}Mn^{III}_3O_3X]^{6+}$ core have also been shown to function as SMMs based on ac magnetic susceptibility measurements.[61−63] One complex in this family, $[Mn_4O_3Cl(O_2CCH_3)_3(dbm)_3]$, where dbm^- is the monoanion of dibenzoylmethane, has been shown to display magnetization hysteresis loops below 0.9 K.[63,64] Recently, a ferric complex, $[Fe_8O_2(OH)_{12}(tacn)_6]^{8+}$, where tacn is triazacyclononane, has been reported to display frequency-dependent out-of-phase (χ''_M) ac magnetic susceptibility peaks[51] and magnetization hysteresis loops.[52] Tetranuclear vanadium butterfly complexes of composition[65] $[V_4O_2(O_2CEt)_7(L)_2]^n$ comprise the fourth family of SMMs, where L is picolinate with $n = -1$ or L is 2,2′-bipyridine with $n = +1$. Frequency-dependent out-of-phase ac magnetic susceptibility signals characteristic of SMMs have been observed for these V_4 butterfly complexes.[65]

For $[Mn_{12}O_{12}(O_2CCH_3)_{16}(H_2O)_4]\cdot 4H_2O\cdot 2HO_2CCH_3$,[4,53] the slow magnetization relaxation has been shown to be due to a $S = 10$ ground-state split by axial zero-field splitting $D\hat{S}_z^2$, where $D = -0.5\ cm^{-1}$. There is a double-well potential-energy curve for reversal of the direction of magnetization for each SMM. The temperature dependence of the time for reversal of the direction of magnetization of each molecule is well described by the Arrhenius law, with an effective activation barrier (U_{eff}) equal to 61−64 K and a preexponential factor (τ_o) equal to $\sim 1 \times 10^7$ Hz.[4,12] The activation barrier is smaller than the thermodynamic barrier, $D\hat{S}_z^2 = 72$ K, expected for an $S = 10$ ground-state split by zero-field interactions with $D = -0.5\ cm^{-1}$. In addition to thermal activation over the barrier, magnetization relaxation occurs via quantum mechanical tunneling through the barrier. The compelling evidence for resonant magnetization tunneling is the observation of steps in the magnetization hysteresis loops occurring at constant intervals of the external magnetic field.[24−27] Calculations for the Mn_{12}Ac SMM have shown that the most likely pathway for quantum magnetization tunneling involves tunneling between the $M_s = \pm 3$ levels.[25b] This explains why the effective energy barrier U_{eff} is smaller than U.

Considerable insight has been obtained from chemical modifications made on the Mn_{12}Ac SMM. Three different types of chemical modifications have been made: (i) The acetate ligands have been replaced by various carboxylate ligands. This modification led to the discovery of isomerism in the Mn_{12} SMMs.[7,60] (ii) It has been possible to reduce or oxidize the Mn_{12} SMMs. Reduction of a Mn_{12} SMM gives anionic $[Mn_{12}O_{12}(O_2CR)_{16}(H_2O)_4]^-$ complexes with a ground-state spin of $S = 19/2$. These reduced Mn_{12} anionic compounds also function as SMMs.[5,66] (iii) Four Mn^{III} ions can be replaced by four Fe^{III} ions leading to a heteronuclear (Fe_4Mn_8) dodecanuclear complex.[67] In this article we present new results for anionic $[Mn_{12}]^-$ complexes.

The feasibility of chemically reducing a Mn_{12} SMM was established by the observation of a reversible one-electron reduction process in the cyclic voltammogram. The salt $(PPh_4)[Mn_{12}O_{12}(O_2CEt)_{16}(H_2O)_4]$ (**1**) was first reported[5] in 1995, and the presence of steps in the magnetization hysteresis loops were noted recently.[68] When the neutral Mn_{12} molecule with a $S = 10$ ground state is reduced by one electron, the spin of the ground state of the anionic complex becomes a half-integer value of $S = 19/2$. One-electron reduction of the core of $[Mn_{12}O_{12}(O_2CEt)_{16}(H_2O)_3]$ leads to a complex with a formal $[Mn^{IV}_4Mn^{III}_7Mn^{II}]$ oxidation level. Half-integer spin complexes are of particular interest because it is predicted that in zero magnetic field magnetization quantum tunneling is not allowed.[69] Recently, a reduced salt with an organic radical cation (m-$MPYNN^+$)$[Mn_{12}O_{12}(O_2CPh)_{16}(H_2O)_4^-]$ was reported, where m-$MPYNN^+$ is m−*N*-methylpyridinium nitronylnitroxide.[70] This salt was reported to have a magnetization relaxation rate that is greater than for a simple Mn_{12} SMM. The detailed characterizations of $(Ph_4P)[Mn_{12}O_{12}(O_2CEt)_{16}(H_2O)_4]$ (**1**) and $(Ph_4P)[Mn_{12}O_{12}\ (O_2CPh)_{16}(H_2O)_4]$ (**2**) are reported in this article.

Experimental Section

Compound Preparation and Physical Measurements. $(PPh_4)[Mn_{12}O_{12}(O_2CEt)_{16}(H_2O)_4]$ (1). This complex was prepared as reported.[5] The purity was confirmed by IR and elemental analysis.

$(PPh_4)[Mn_{12}O_{12}(O_2CPh)_{16}(H_2O)_4]$ (2). Ligand substitution of $[Mn_{12}O_{12}(O_2CMe)_{16}(H_2O)_4]\cdot 4(H_2O)\cdot 2(HO_2CMe)$ or Mn_{12}Ac lead to complex **2**. Mn_{12}Ac was prepared as reported.[10] To a 50-mL CH_2Cl_2 solution of Mn_{12}Ac (1.0 g, 0.485 mmol) HO_2CPh (1.78 g, 14.6 mmol) was added. The mixture was stirred overnight and then concentrated to remove acetic acid by vacuum distillation. The resulting solid and additional HO_2CPh (1.78 g, 14.6 mmol) were dissolved in CH_2Cl_2 (50 mL), stirred overnight, and then concentrated to remove acetic acid again. To fully substitute the acetate ligands, this second step was repeated. The resulting brown powder was dissolved in CH_2Cl_2 and layered with hexanes. Slow diffusion of the layers yielded dark brown crystals of $[Mn_{12}O_{12}(O_2CPh)_{16}(H_2O)_4]$ (**3**) (93% yield based on total available Mn_{12}Ac). The crystals were washed on a frit with hexanes.

Solid PPh_4I (0.05 g 0.105 mmol) was added, to a stirred dark brown solution of the benzoate complex **3** (0.3 g, 0.105 mmol) in CH_2Cl_2 (20 mL). The solution was stirred for an additional 45 min with no noticeable color change. A mixed solvent of EtOAc/Et_2O, (2:1, 100

(57) Schake, A. R.; Tsai, H.-L.; de Vries, N.; Webb, R. J.; Folting, K.; Hendrickson, D. N.; Christou, G. *J. Chem. Soc., Chem. Commun.* **1992**, 181.

(58) Sessoli, R.; Tsai, H.-L.; Schake, A. R.; Wang, S.; Vincent, J. B.; Folting, K.; Gatteschi, D.; Christou, G.; Hendrickson, D. N. *J. Am. Chem. Soc*. **1993**, *115*, 1804.

(59) Ruiz. D.; Sun, Z.; Albela, B.; Folting, K.; Ribas, J.; Christou, G.; Hendrickson, D. N. *Angew. Chem., Int. Ed*. **1998**, *37*, 300.

(60) Aubin, S. M. J.; Sun, Z.; Guzei, I. A.; Rheingold, A. L.; Christou, G.; Hendrickson, D. N., *Chem. Commun*. **1997**, 2239.

(61) (a) Hendrickson, D. N.; Christou, G.; Schmitt, E. A.; Libby, E.; Bashkin, J. S.; Wang, S.; Tsai, H.-L.; Vincent, J. B.; Boyd, P. D. W.; Huffman, J. C.; Folting, K.; Li, Q.; Streib, W. E. *J. Am. Chem. Soc*. **1992**, *114*, 2455. (b) Wemple, M. W.; Adams, D. M.; Folting, K.; Hendrickson, D. N.; Christou, G. *J. Am. Chem. Soc*. **1995**, *117*, 7275. (c) Wemple, M. W.; Adams, D. M.; Hagen, K. S.; Folting, K.; Hendrickson, D. N.; Christou, G. *J. Chem. Soc., Chem. Commun*. **1995**, 1591. (d) Wang, S.; Folting, K.; Streib, W. E.; Schmitt, E. A.; McCusker, J. K.; Hendrickson, D. N.; Christou, G. *Angew. Chem., Int. Ed. Engl*. **1991**, *30*, 305. (e) Wang, S.; Tsai, H.-L.; Streib, W. E.; Christou, G.; Hendrickson, D. N. *Chem. Soc., Chem. Commun.* **1992**, 1427. (f) Wang, S.; Tsai, H.-L.; Libby, E.; Folting, K.; Streib, W. E.; Hendrickson, D. N.; Christou, G. *Inorg. Chem*. **1996**, *35*, 7578.

(62) Wemple, M. W.; Tsai, H.-L.; Folting, K.; Hendrickson, D. N.; Christou, G. *Inorg. Chem*. **1993**, *32*, 2025.

(63) Aubin, S. M. J.; Dilley, N. R.; Wemple, M. W.; Maple, M. B.; Christou, G.; Hendrickson, D. N. *J. Am. Chem. Soc*. **1998**, *120*, 839.

(64) Aubin, S. M. J.; Dilley, N. R.; Pardi, L.; Krzystek, J.; Wemple, M. W.; Brunel, L.-C.; Maple, M. B.; Christou, G.; Hendrickson, D. N. *J. Am. Chem. Soc*. **1998**, *120*, 4991.

(65) (a) Sun, Z.; Graig, C. M.; Castro, S. L.; Hendrickson, D. N.; Christou, G. *J. Chem. Soc., Chem. Common.* **1998**, 721. (b) Castro, S. L.; Sun, Z.; Grant, M. G.; Bollinger, J. C.; Hendrickson, D. N.; Christou, G. *J. Am. Chem. Soc*. **1998**, *120*, 2365.

(66) Tsai, H.-L.; Eppley, H. J.; de Vries, N.; Folting, K.; Christou, G.; Hendrickson, D. N. *J. Chem. Soc., Chem. Commun*. **1994**, 1746.

(67) Schake, A. R.; Tsai, H.-L.; Webb, R. J.; Folting, K.; Christou, G.; Hendrickson, D. N. *Inorg. Chem*. **1994**, *33*, 6020.

(68) (a) Aubin, S. M. J.; Spagna, S.; Eppley, H. J.; Sager, R. E.; Christou, G. Hendrickson, D. N. *J. Chem. Soc., Chem. Common*. **1998**, 803. (b) Aubin, S. M. J.; Spagna, S.; Eppley, H. J.; Sager, R. E.; Folting, K.; Christou, G.; Hendrickson, D. N. *Mol. Cryst. Liq. Cryst*. **1997**, *305*, 181.

(69) (a) Loss, D.; Di Vincenzo, D. P.; Grinstein, G.; Awschalom, D.; Smyth, J. F. *Physica B* **1993**, *189*, 189. (b) Di Vincenzo, D. P. *Physica B* **1994**, *197*, 109.

(70) Takeda, K.; Awaga, K. *Phys. Rev. B* **1997**, *56*, 14560.

mL) was added to give a dark brown precipitate which was collected by filtration, washed well with EtOAc and Et_2O and dried in vacuo. The yield was ~78%. X-ray quality needle crystals were obtained by layering a CH_2Cl_2 solution with hexanes. Elemental analysis: Calcd (Found) for $C_{136}H_{108}O_{48}Mn_{12}P$: C, 51.02 (51.16); H, 3.4 (3.46) with the composition of **(**PPh_4)$[Mn_{12}O_{12}(O_2CPh)_{16}(H_2O)_4]$. The composition obtained from the single-crystal X-ray structure is the salt molecule with either $5CH_2Cl_2$ or $8CH_2Cl_2$ solvate molecules, i.e., complex **2**·$5CH_2Cl_2$ or **2**·$8CH_2Cl_2$ (vide infra). The solvate molecules were lost on drying before the elemental analysis was performed.

Physical Measurements. Direct current magnetic susceptibility data were collected on microcrystalline samples of $PPh_4[Mn_{12}O_{12}(O_2CPh)_{16}(H_2O)_4]$ (**2**) or a single-crystal sample restrained in eicosane to prevent torquing on a Quantum Design MPMS SQUID magnetometer equipped with a 5.5-T magnet. A diamagnetic correction to the observed susceptibilities was applied using Pascal's constants. Alternating current susceptibility measurements were carried out on a Quantum Design MPMS2 SQUID magnetometer equipped with a 1-T magnet and capable of achieving temperatures of 1.7−400 K. The ac field range is 1×10^{-4} to 5 Oe, oscillating at a frequency in the range of 5×10^{-4} to 1512 Hz. One set of ac susceptibility data was collected for a powdered, microcrystalline sample in an ac field of 1.0 Oe, oscillating in the 250−1000 Hz range. The other data sets were measured on microcrystalline samples aligned in eicosane with a variable applied dc field (0−10.0 kOe) and at various temperatures. Sample alignments in eicosane were performed while keeping the samples in a 5.5-T field at a temperature above the melting point (308−312 K) of eicosane for 15 min, after which the temperature was gradually decreased below the melting point to solidify the eicosane to constrain the sample. Thus at room temperature, the little crystals are frozen in an orientation such that the axial magnetic anisotropic axis of each crystal is parallel to one another.

HFEPR measurements were collected on complex **1** at the National High Magnetic Field Laboratory, Florida State University, Tallahassee, Florida. The HFEPR spectrometer is capable of fields up to 14.5 T in the temperature range of 1.7−300 K and is equipped with a general Gunn effect diode source for generating high-frequency microwaves. The operating frequency range is 110−550 GHz. Frequencies between 220 and 550 GHz were obtained by using a solid-state harmonic generator that multiplies the fundamental frequency (i.e., 110 GHz) and high-pass filters to filter out the lower frequency harmonics. The field was swept at a rate of 0.5 T/min or 0.3 T/min in the 0−13 T range and 0.3 T/min in the 13−14.5 T range. Data were collected on a microcrystalline sample of complex **1**. Because of the large external field and the sample's predisposition to orient in a field, the resulting EPR data are pseudo−single-crystal spectra, where the microcrystals are oriented with their easy axis parallel to the external magnetic field.

Crystallographic Structural Determination for Complex 2. X-ray diffraction data were collected on a crystal of $PPh_4[Mn_{12}O_{12}(O_2CPh)_{16}(H_2O)_4]$·$(5CH_2Cl_2)$ with a modified four-circle Picker diffractometer; details of the diffractometer, low-temperature facilities, and computation procedures used by the Molecular Structure Center at Indiana University are available elsewhere.[71] The structure of complex **2**·$(5CH_2Cl_2)$ was solved using direct methods, completed by subsequent difference Fourier synthesis, and refined by full-matrix least-squares procedures. To minimize solvate molecule loss, crystals were pipetted from the mother liquor into a Petri dish precooled with dry ice. A suitable single crystal was selected, affixed to a glass fiber with silicone grease, and transferred to the goniostat where it was cooled for characterization and data collection. Crystallographic data are shown in Table 1. The X-ray structures were solved using a combination of direct methods (SHELXS-86) and difference Fourier techniques and refined by a full-matrix least squares refinement. The positions of the 12 manganese atoms were obtained from the best solution and the remaining nonhydrogen atoms were located in many iterations of least-squares refinement, followed by a difference Fourier calculation. It was difficult to locate many of the atoms in the ligands oriented perpendicular to the main Mn_{12} plane. Two phenyl rings [C(41) through C(46) and C(50) through C(55)] were obtained by joining two phenyl rings together based on the observed peaks. The fitted atoms were not refined further. An attempt to refine these atoms resulted in thermal parameters above 4.0. One phenyl ring [C(59) to C(63)] is missing an atom. The atoms in the phenyl rings on the teraphenylphosphonium cation failed to refine properly and were eventually refined as fixed units. Additional disorder involving the water molecules and bridging benzoates was found. The disorder at atoms Mn(8), Mn(9), and Mn(10) is reasonably well defined, so that O(27) and O(118) are either H_2O or part of the bridging benzoate group. In the disorder at Mn(5), Mn(6), and Mn(12), it was not possible to locate two distinct phenyl groups.

Table 1. Crystallographic Data for $(Ph_4P)[Mn_{12}O_{12}(O_2CPh)_{16}(H_2O)_4]$·$n(CH_2Cl_2)$ (**2**)

	2·$5CH_2Cl_2$	**2**·$8CH_2Cl_2$
empirical formula	$C_{141}H_{118}Cl_{10}Mn_{12}O_{48}P$	$C_{144}H_{122}Cl_{16}Mn_{12}O_{47}P$
fw, g/mol[a]	3625.22	3861.87
space group	$P\bar{1}$	$P\bar{1}$
a, Å	18.081(10)	17.2329(2)
b, Å	26.406(15)	17.8347(2)
c, Å	17.191(11)	26.8052(2)
α, deg	93.84(3)	90.515(2)
β, deg	102.89(3)	94.242 (2)
γ, deg	89.03(3)	101.437(2)
V, Å^3	7982.91	8050.34
Z	2	2
T, K	105	213
λ, Å[b]	0.710 69	0.710 73
ρ_{calc}, g/cm^3	1.508	1.593
R (R_w)[c,d]	0.1460 (0.1520)	10.54 (14.02)

[a] Including solvate molecules. [b] Graphite monochromator. [c] $R = \Sigma F_o| - |F_c||/\Sigma|F_o|$. [d] $R_w = [\Sigma w(|F_o| - |F_c|)^2/w|F_o|^2]^{1/2}$, where $w = 1/s^2|F_o|$. [e] $gof = [\Sigma w(|F_o| - |F_c|)^2]/(n - p)]1/2$; *n* is the number of observed reflections, *p* is the number of refined parameters.

An attempt to improve the structural resolution was made by using a $P4/CCD$ diffractometer at the University of Delaware. Data were collected on a single crystal of complex **2**, and the same space group ($P\bar{1}$) and similar unit parameters were obtained (see Table 1). Independent studies (chemical analyses) found that complex **2** loses CH_2Cl_2 solvate molecules. The initial crystal studied at Indiana University had a composition of **2**·$5CH_2Cl_2$, whereas the crystal studied at the University of Delaware had a composition of **2**·$8CH_2Cl_2$. There are three more CH_2Cl_2 solvate molecules than in the first X-ray structure. The same disorders of phenyl rings and solvate molecules were found, which kept the *R* factor at 10.54%.

Results and Discussion

Description of the Structure. Complex **2**·$8(CH_2Cl_2)$ crystallizes in the $P\bar{1}$ space group. Crystallographic data are given in Table 1, and selected bond distances and angles in Tables 2 and 3, respectively. The structure shows PPh_4^+ cations and $[Mn_{12}O_{12}(O_2CC_6H_5)_{16}(H_2O)_4]^-$ anions. Plots of the anion and a stereoview of the molecular arrangement in the unit cell are shown in Figures 1 and 2. In general, the anion is similar in many aspects to the previously structurally characterized[5] anion of $[Mn_{12}O_{12}(O_2CEt)_{16}(H_2O)_4]^-$. The $[Mn_{12}O_{12}]^{16+}$ core of the anion is formed of an external ring of eight Mn atoms and an internal tetrahedron of four Mn atoms. It is difficult to determine the valence of each manganese atom based on the bond valence sum analysis and Jahn−Teller distortion of Mn^{III} ions because of the disorder in the phenyl rings and solvate molecules.

A bond valence sum is an empirical value, based on crystallographically determine metal−ligand bond distances, that may be used to determine the oxidation state of a metal ion in a molecule. Bond valence sums(s) are calculated using eq 1,

$$s = \exp[(r_0 - r)/B] \quad (1)$$

where *r* is the observed bond length, and r_0 and *B* are empirically

(71) Chisholm, M. F.; Folting, K.; Huffman, J. C.; Kiirkpatrick, D. C. *Inorg. Chem.* **1994**, *23*, 1021.

Table 2. Bond Distances for $(PPh_4)[Mn_{12}O_{12}(O_2CPh)_{16}(H_2O)_4]\cdot 8CH_2Cl_2$ (Complex 2) at 105 K

A	B	distance	A	B	distance
Mn(1)	O(12)	1.861(5)	Mn(7)	O(7)	1.850(5)
Mn(1)	O(11)	1.864(5)	Mn(7)	O(6)	1.900(5)
Mn(1)	O(2)	1.882(5)	Mn(7)	O(23)	1.953(7)
Mn(1)	O(3)	1.893(5)	Mn(7)	O(16)	1.941(6)
Mn(1)	O(1)	1.918(6)	Mn(7)	O(18)	2.143(8)
Mn(1)	O(41)	1.949(7)	Mn(7)	O(21)	2.146(7)
Mn(2)	O(5)	1.863(5)	Mn(8)	O(7)	1.864(5)
Mn(2)	O(6)	1.883(5)	Mn(8)	O(8)	1.897(6)
Mn(2)	O(4)	1.886(5)	Mn(8)	O(25)	1.930(6)
Mn(2)	O(1)	1.893(5)	Mn(8)	O(24)	1.956(6)
Mn(2)	O(2)	1.910(6)	Mn(8)	O(27)	2.160(10)
Mn(2)	O(20)	1.937(7)	Mn(8)	O(22)	2.197(8)
Mn(3)	O(7)	1.849(5)	Mn(9)	O(8)	1.920(6)
Mn(3)	O(8)	1.880(6)	Mn(9)	O(26)	1.964(7)
Mn(3)	O(3)	1.904(5)	Mn(9)	O(30)	2.005(6)
Mn(3)	O(2)	1.918(5)	Mn(9)	O(32)	2.175(9)
Mn(3)	O(28)	1.911(9)	Mn(9)	O(29)	2.235(8)
Mn(3)	O(4)	2.003(6)	Mn(10)	O(9)	1.855(6)
Mn(4)	O(9)	1.839(5)	Mn(10)	O(10)	1.883(5)
Mn(4)	O(10)	1.897(5)	Mn(10)	O(31)	1.924(6)
Mn(4)	O(4)	1.914(5)	Mn(10)	O(35)	1.943(6)
Mn(4)	O(1)	1.917(5)	Mn(10)	O(37)	2.192(10)
Mn(4)	O(3)	1.921(7)	Mn(10)	O(33)	2.209(9)
Mn(4)	O(38)	1.950(8)	Mn(11)	O(11)	1.860(5)
Mn(5)	O(5)	1.879(6)	Mn(11)	O(10)	1.879(6)
Mn(5)	O(12)	1.884(6)	Mn(11)	O(36)	1.938(6)
Mn(5)	O(13)	1.939(6)	Mn(11)	O(39)	1.964(7)
Mn(5)	O(45)	1.982(6)	Mn(11)	O(34)	2.188(8)
Mn(5)	O(47)	2.079(7)	Mn(11)	O(43)	2.264(8)
Mn(6)	O(6)	1.878(5)	Mn(12)	O(12)	1.868(6)
Mn(6)	O(5)	1.905(5)	Mn(12)	O(11)	1.875(5)
Mn(6)	O(15)	1.943(6)	Mn(12)	O(44)	1.924(6)
Mn(6)	O(14)	1.943(5)	Mn(12)	O(40)	1.942(6)
Mn(6)	O(17)	2.140(8)	Mn(12)	O(42)	2.123(9)
Mn(6)	O(19)	2.196(7)	Mn(12)	O(46)	2.215(7)

determined parameters. Values for s are given in Table 4 for Mn^{n+} ($n = 2, 3, 4$). Bond sum analyses have been used to verify oxidation states in metalloenzymes and superconductors,[72c] and in $[Mn_{13}O_8(OEt)_6(O_2CPh)_{12}]$, a compound having Mn atoms in three different oxidation states [six Mn^{II}, six Mn^{III}, and one Mn^{IV}].[73]

As seen in Table 4, bond valence sums for complex **2** indicate that it is difficult to determine the valence of each manganese ion probably because of all the elements of disorder in the complex. For the four atoms in the central cubane [Mn(1), Mn(2), Mn(3), and Mn(4)] the calculated values tend to be $s = 4$ for Mn^{IV}. Three of these values are a little lower than 4, but it is clear that this central cubane unit is composed of Mn^{IV} ions, that is the cubane unit is $[Mn_4O_4]^{8+}$. The other eight Mn atoms are bonded to the four Mn^{IV} cubane atoms by μ_3−O^{2-} ions. For these eight Mn atoms, seven of the calculated values of s range from 3.2 to 3.4 for Mn^{III} and only one value is at 3.0. In a formal sense, these eight Mn atoms could be valence trapped as $Mn^{III}_7Mn^{II}$ or the valences could be electronically delocalized. From the s values given in Table 4 it is not possible to pick between these limiting descriptions. On the other hand, the bond valence sum analysis gave a conclusive result for the anion in complex **1**. In that case,[5] the extra electron resides only on one Mn atom of the eight ring Mn^{III} ions. Thus, it was found that the valences for complex **1** are $Mn^{IV}_4Mn^{III}_7Mn^{II}$. This was also supported by the pronounced Jahn−Teller elongation of Mn^{III}−O bond found for seven of the Mn atoms. A Mn^{III} ion, rather than a core Mn^{IV} ion, is reduced to a Mn^{II} ion in complex **1**,[5] because for a Mn^{IV} ion to become reduced, it must undergo significant structural rearrangement, since Jahn−Teller distortion is expected for a high-spin Mn^{III} ion. However, a Jahn−Teller distorted Mn^{III} ion in the cubane core would create strain in the apparently rigid $[Mn_4O_4]$ cubane unit. In contrast, with the electron trapped on an outer Mn atom of the ring, where the bonding framework is less rigid, the additonal equatorial elongation on one outer Mn atom would not perturb the basic $[Mn_{12}O_{12}]$ structure significantly.

Before the structural characterization of $\mathbf{2}\cdot 8(CH_2Cl_2)$ above, another crystal was measured at Indiana University. This crystal refined as $\mathbf{2}\cdot 5C(H_2Cl_2)$; however, as seen in Table 1, the space group is the same and the unit cell parameters are similar to those for the first crystal. The same disorder of ligands and solvate molecules were found. This structure is not as good as the other one because of partial loss of the CH_2Cl_2 solvate molecules. Details of both structures are available in the Supporting Material.

HFEPR Spectroscopy. HFEPR is useful to characterize molecules with large-spin ground states and considerable magnetic anisotropy ($D\hat{S}_z^2$). HFEPR data have been reported[53] for $Mn_{12}Ac$. The advantage of HFEPR over magnetization vs field data is that the ground state can be probed directly. Peaks observed in high-field HFEPR spectra are due to transitions between sublevels of the ground and low-energy states. Magnetization vs field data reflect averages and are not nearly as discriminating in defining spin Hamiltonian parameters. In HFEPR spectra Boltzmann populations are reflected in the relative intensities of peaks. At low temperatures only a few sublevels of the ground state are populated, and therefore only a few peaks are seen in the EPR spectrum. As temperature is increased and more states become populated, more peaks are observed in the spectrum.

The ground state of a SMM is split by axial zero-field splitting, and the spin Hamiltonian can be expressed in its simplest form as given in eq 2:

$$\hat{H} = g\mu_B\hat{H}\cdot\hat{S} + D[\hat{S}_z^2 - {}^1/_3S(S+1)] \qquad (2)$$

where μ_B is the Bohr magneton and g is Lande's factor. The first term is the Zeeman term, and the second interaction is the axial zero-field interaction. The parameter D gauges the axial zero-field splitting of the ground state. If the axial anisotropy axis (i.e., z-axis) of the molecules are oriented parallel to an external field H, then the energy of each M_s sublevel of the ground state is given as $E = M_s g\mu_B H + D[M_s - {}^1/_3S(S+1)]$.

Complexes **1** and **2** have a large-spin ($S = 19/2$) ground state, thus EPR experiments carried out at conventional frequencies (e.g., X-band at ~9 GHz) are useless. It takes much higher frequencies to see EPR transitions for these magnetically anisotropic high-spin molecules. HFEPR spectra can be used to determine both the magnitude and *sign* of the zero-field splitting parameter D. If $D < 0$ for an $S = 19/2$ molecule, then in zero field the $M_s = \pm 19/2$ levels are energetically degenerate and lie at the lowest energy. Allowed, $\Delta M_s = \pm 1$, transitions can be seen between the M_s and $M_s + 1$ levels, leading to "fine structure" in the HFEPR spectrum. The temperature dependence of the peak intensities for a fine structure group of peaks indicates the sign of the D parameter. If the lowest field peak

(72) (a) Brown, I. D. *Solid State Chem.* **1989**, *82*, 122. (b) Thorpe, H. H. *Inorg. Chem.* **1992**, *32*, 1585. (c) Brown, I. D.; Altermatt, D. *Acta Crystallogr. Sect. B* **1985**, *412*, 244.
(73) Sun, Z.; Gantzel, P. K.; Hendrickson, D. N. *Inorg. Chem.* **1996**, *35*, 6640.

Table 3. Selected Bond Angles for $(PPh_4)[Mn_{12}O_{12}(O_2CPh)_{16}(H_2O)_4]\cdot 5CH_2Cl_2$ (Complex **2**) at 105 K

A	B	C	angle	A	B	C	angle	A	B	C	angle	A	B	C	angle
O(12)	Mn(1)	O(11)	83.9(2)	O(1)	Mn(2)	O(2)	83.6(2)	O(8)	Mn(8)	O(24)	174.6(4)	O(9)	Mn(10)	O(31)	95.3(3)
O(12)	Mn(1)	O(2)	96.4(2)	O(5)	Mn(2)	O(20)	92.5(3)	O(25)	Mn(8)	O(24)	86.1(3)	O(10)	Mn(10)	O(31)	174.1(4)
O(11)	Mn(1)	O(2)	172.3(3)	O(6)	Mn(2)	O(20)	91.2(3)	O(7)	Mn(8)	O(27)	89.0(3)	O(9)	Mn(10)	O(35)	173.5(4)
O(12)	Mn(1)	O(3)	175.6(3)	O(4)	Mn(2)	O(20)	89.7(3)	O(8)	Mn(8)	O(27)	86.8(3)	O(10)	Mn(10)	O(35)	93.7(2)
O(11)	Mn(1)	O(3)	97.8(2)	O(1)	Mn(2)	O(20)	94.6(3)	O(25)	Mn(8)	O(27)	89.6(4)	O(31)	Mn(10)	O(35)	86.2(3)
O(2)	Mn(1)	O(3)	81.4(2)	O(2)	Mn(2)	O(20)	175.1(2)	O(24)	Mn(8)	O(27)	88.0(3)	O(9)	Mn(10)	O(37)	85.4(3)
O(12)	Mn(1)	O(1)	91.4(2)	O(7)	Mn(3)	O(8)	83.9(2)	O(7)	Mn(8)	O(22)	92.0(3)	O(10)	Mn(10)	O(37)	85.2(3)
O(11)	Mn(1)	O(1)	88.6(3)	O(7)	Mn(3)	O(3)	172.3(2)	O(8)	Mn(8)	O(22)	95.4(3)	O(31)	Mn(10)	O(37)	88.9(4)
O(2)	Mn(1)	O(1)	83.7(2)	O(8)	Mn(3)	O(3)	101.3(2)	O(25)	Mn(8)	O(22)	89.5(3)	O(35)	Mn(10)	O(37)	88.3(3)
O(3)	Mn(1)	O(1)	84.6(2)	O(7)	Mn(3)	O(2)	93.7(2)	O(24)	Mn(8)	O(22)	89.8(3)	O(9)	Mn(10)	O(33)	93.4(3)
O(12)	Mn(1)	O(41)	92.4(3)	O(8)	Mn(3)	O(2)	170.2(3)	O(27)	Mn(8)	O(22)	177.7(3)	O(10)	Mn(10)	O(33)	94.7(3)
O(11)	Mn(1)	O(41)	91.6(3)	O(3)	Mn(3)	O(2)	80.2(2)	O(8)	Mn(9)	O(9)	94.5(2)	O(31)	Mn(10)	O(33)	91.3(4)
O(2)	Mn(1)	O(41)	96.2(3)	O(7)	Mn(3)	O(28)	93.0(3)	O(8)	Mn(9)	O(26)	90.2(3)	O(35)	Mn(10)	O(33)	92.9(3)
O(3)	Mn(1)	O(41)	91.7(3)	O(8)	Mn(3)	O(28)	92.5(3)	O(9)	Mn(9)	O(26)	174.8(3)	O(37)	Mn(10)	O(33)	178.8(3)
O(1)	Mn(1)	O(41)	176.2(3)	O(3)	Mn(3)	O(28)	92.4(3)	O(8)	Mn(9)	O(30)	175.8(2)	O(11)	Mn(11)	O(10)	94.9(2)
O(5)	Mn(2)	O(6)	84.8(2)	O(2)	Mn(3)	O(28)	97.1(3)	O(9)	Mn(9)	O(30)	89.7(3)	O(11)	Mn(11)	O(36)	173.5(3)
O(5)	Mn(2)	O(4)	175.8(2)	O(7)	Mn(3)	O(4)	91.8(3)	O(26)	Mn(9)	O(30)	85.6(3)	O(10)	Mn(11	O(36)	91.4(3)
O(6)	Mn(2)	O(4)	98.8(2)	O(8)	Mn(3)	O(4)	88.4(3)	O(8)	Mn(9)	O(32)	90.5(3)	O(11)	Mn(11)	O(39)	90.3(3)
O(5)	Mn(2)	O(1)	95.5(2)	O(3)	Mn(3)	O(4)	82.8(2)	O(9)	Mn(9)	O(32)	94.2(3)	O(10)	Mn(11)	O(39)	173.6(3)
O(6)	Mn(2)	O(1)	174.2(3)	O(2)	Mn(3)	O(4)	82.2(2)	O(26)	Mn(9)	O(32)	87.9(3)	O(36)	Mn(11)	O(39)	83.2(3)
O(4)	Mn(2)	O(1)	80.8(2)	O(28)	Mn(3)	O(4)	175.2(3)	O(30)	Mn(9)	O(32)	89.1(3)	O(11)	Mn(11)	O(34)	90.0(3)
O(5)	Mn(2)	O(2)	92.2(2)	O(9)	Mn(4)	O(10)	84.2(2)	O(8)	Mn(9)	O(29)	91.9(3)	O(10)	Mn(11)	O(34)	95.2(3)
O(6)	Mn(2)	O(2)	90.6(2)	O(9)	Mn(4)	O(4)	96.3(2)	O(9)	Mn(9)	O(29)	88.1(3)	O(36)	Mn(11)	O(34)	90.9(3)
O(4)	Mn(2)	O(2)	85.5(2)	O(10)	Mn(4)	O(4)	173.7(3)	O(26)	Mn(9)	O(29)	89.7(3)	O(39)	Mn(11)	O(34)	88.5(3)
O(9)	Mn(4)	O(1)	173.3(3)	O(15)	Mn(6)	O(14)	84.9(2)	O(30)	Mn(9)	O(29)	88.3(3)	O(11)	Mn(11)	O(43)	91.5(3)
O(10)	Mn(4)	O(1)	99.5(2)	O(6)	Mn(6)	O(17)	94.5(3)	O(10)	Mn(11)	O(43)	90.1(3)	Mn(3)	O(3)	Mn(4)	96.9(3)
O(4)	Mn(4)	O(1)	79.4(2)	O(5)	Mn(6)	O(17)	86.7(3)	O(36)	Mn(11)	O(43)	87.0(3)	Mn(2)	O(4)	Mn(4)	100.1(2)
O(9)	Mn(4)	O(3)	90.7(3)	O(15)	Mn(6)	O(17)	100.1(3)	O(39)	Mn(11)	O(43)	86.0(3)	Mn(2)	O(4)	Mn(3)	94.3(2)
O(10)	Mn(4)	O(3)	89.0(3)	O(14)	Mn(6)	O(17)	88.9(3)	O(34)	Mn(11)	O(43)	174.3(3)	Mn(4)	O(4)	Mn(3)	93.9(3)
O(4)	Mn(4)	O(3)	84.8(2)	O(6)	Mn(6)	O(19)	87.1(2)	O(12)	Mn(12)	O(11)	83.4(2)	Mn(2)	O(5)	Mn(5)	132.3(3)
O(1)	Mn(4)	O(3)	83.8(2)	O(5)	Mn(6)	O(19)	86.5(2)	O(12)	Mn(12)	O(44)	94.9(2)	Mn(2)	O(5)	Mn(6)	94.8(2)
O(9)	Mn(4)	O(38)	92.9(3)	O(15)	Mn(6)	O(19)	86.7(2)	O(11)	Mn(12)	O(44)	177.1(3)	Mn(5)	O(5)	Mn(6)	124.9(3)
O(10)	Mn(4)	O(38)	89.9(3)	O(14)	Mn(6)	O(19)	89.5(2)	O(12)	Mn(12)	O(40)	177.7(3)	Mn(6)	O(6)	Mn(2)	95.1(2)
O(4)	Mn(4)	O(38)	96.3(3)	O(17)	Mn(6)	O(19)	172.8(3)	O(11)	Mn(12)	O(40)	95.2(2)	Mn(6)	O(6)	Mn(7)	121.2(3)
O(1)	Mn(4)	O(38)	92.7(3)	O(7)	Mn(7)	O(6)	94.8(2)	O(44)	Mn(12)	O(40)	86.5(3)	Mn(2)	O(6)	Mn(7)	130.5(3)
O(3)	Mn(4)	O(38)	176.1(3)	O(7)	Mn(7)	O(23)	89.9(3)	O(12)	Mn(12)	O(42)	86.0(3)	Mn(7)	O(7)	Mn(3)	133.7(3)
O(5)	Mn(5)	O(12)	95.9(2)	O(6)	Mn(7)	O(23)	175.3(3)	O(11)	Mn(12)	O(42)	87.8(3)	Mn(7)	O(7)	Mn(8)	127.4(3)
O(5)	Mn(5)	O(13)	92.5(3)	O(7)	Mn(7)	O(16)	170.3(2)	O(44)	Mn(12)	O(42)	89.8(3)	Mn(3)	O(7)	Mn(8)	96.5(2)
O(12)	Mn(5)	O(13)	167.3(3)	O(6)	Mn(7)	O(16)	92.9(3)	O(40)	Mn(12)	O(42)	92.2(3)	Mn(3)	O(8)	Mn(8)	94.3(3)
O(5)	Mn(5)	O(45)	168.2(3)	O(23)	Mn(7)	O(16)	82.5(3)	O(12)	Mn(12)	O(46)	93.4(3)	Mn(3)	O(8)	Mn(9)	131.0(3)
O(12)	Mn(5)	O(45)	88.0(3)	O(7)	Mn(7)	O(18)	94.0(3)	O(11)	Mn(12)	O(46)	91.7(3)	Mn(8)	O(8)	Mn(9)	129.1(3)
O(13)	Mn(5)	O(45)	82.0(3)	O(6)	Mn(7)	O(18)	93.4(3)	O(44)	Mn(12)	O(46	90.7(3)	Mn(4)	O(9)	Mn(10)	96.7(3)
O(5)	Mn(5)	O(47)	94.0(3)	O(23)	Mn(7)	O(18)	86.0(3)	O(40)	Mn(12)	O(46)	88.4(3)	Mn(4)	O(9)	Mn(9)	132.9(3)
O(12)	Mn(5)	O(47)	97.0(2)	O(16)	Mn(7)	O(18)	91.5(3)	O(42)	Mn(12)	O(46)	179.3(3)	Mn(10)	O(9)	Mn(9)	126.8(3)
O(13)	Mn(5)	O(47)	91.9(3)	O(7)	Mn(7)	O(21)	90.6(3)	Mn(2)	O(1)	Mn(4)	99.7(2)	Mn(11)	O(10)	Mn(10)	126.2(3)
O(45)	Mn(5)	O(47)	96.6(3)	O(6)	Mn(7)	O(21)	91.2(3)	Mn(2)	O(1)	Mn(1)	95.4(3)	Mn(11)	O(10)	Mn(4)	131.1(3)
O(6)	Mn(6)	O(5)	83.7(2)	O(23)	Mn(7)	O(21)	89.1(3)	Mn(4)	O(1)	Mn(1)	94.6(3)	Mn(10)	O(10)	Mn(4)	93.8(2)
O(6)	Mn(6)	O(15)	94.5(2)	O(16)	Mn(7)	O(21)	83.3(3)	Mn(1)	O(2)	Mn(3)	99.1(2)	Mn(11)	O(11)	Mn(1)	131.8(3)
O(5)	Mn(6)	O(15)	173.1(3)	O(18)	Mn(7)	O(21)	173.2(2)	Mn(1)	O(2)	Mn(2)	96.0(3)	Mn(11)	O(11)	Mn(12)	131.9(3)
O(6)	Mn(6)	O(14)	176.6(3)	O(7)	Mn(8)	O(8)	83.1(2)	Mn(3)	O(2)	Mn(2)	96.3(3)	Mn(1)	O(11)	Mn(12)	95.5(2)
O(5)	Mn(6)	O(14)	96.5(2)	O(7)	Mn(8)	O(25)	177.8(3)	Mn(1)	O(3)	Mn(3)	99.2(2)	Mn(1)	O(12)	Mn(12)	95.8(2)
O(8)	Mn(8)	O(25)	95.2(3)	O(32)	Mn(9)	O(29)	176.6(3)	Mn(1)	O(3)	Mn(4)	95.3(3)	Mn(1)	O(12)	Mn(5)	132.2(3)
O(7)	Mn(8)	O(24)	95.5(2)	O(9)	Mn(10	-O(10)	84.2(2)					Mn(12)	O(12)	Mn(5)	122.9(3)

in the fine structure becomes the most intense as the sample temperature is decreased, then the D value is negative. Such a direct determination of the sign of D, and for that matter the magnitude of D, is not readily possible through an analysis of magnetization vs field data for a polycrystalline sample.

HFEPR data were collected for a microcrystalline sample of complex **1** at frequencies between 220 and 550 GHz and temperatures between 5 and 30 K. The Hamiltonian that best fits the HFEPR data for complex **1** is given as

$$\hat{H} = g\mu_B \hat{H}\cdot\hat{S} + D[\hat{S}_z^2 - {}^1/_3 S(S+1)] + B_4^0 \hat{\mathbf{O}}_4^0 \qquad (3)$$

where $\hat{\mathbf{O}}_4^0 = 35\hat{\mathbf{S}}_z^4 - 30S(S+1)\hat{\mathbf{S}}_z^2 + 25\hat{\mathbf{S}}_z^2 + 6S(S+1)$. The last term in this Hamiltonian is the axial quartic zero-field term. Because we are in the high-field limit [$g\mu_B H_o \gg (2|M_s| - 1)$, where $g\mu_B H_o = h\nu$ and H_o is the resonance field of a free electron], then transitions will occur at the following field values:

$$H_r(M_s) = g_e/g\,[H_o - (2M_s+1)(D' + 25B_4^{0'} - 30S(S+1)B_4^{0'}) - 35B_4^{0'}(4M_s^3 + 6M_s^2 + 4M_s + 1)] \quad (4)$$

where $D' = [(3\cos^2\theta - 1)D]/2g_e\mu_B$, $B_4^{0'} = [(3\cos^2\theta - 1)B_4^0]/2g_e\mu_B$ and θ is the angle between the external field and the anisotropy axis for an individual molecule.

Because of the large magnetoanisotropy in these molecules microcrystals readily orient in the field and the resulting HFEPR spectra are thus pseudo−single-crystal spectra. In other words, if the z-axis of all the molecules in the crystal unit cell are parallel to one another, then the angle (θ) between the z-axis of the molecule(s) and the external field axis is zero. However, this is not the case for complex **1**. $(PPh_4)[Mn_{12}O_{12}(O_2CEt)_{16}(H_2O)_4]$ (**1**) crystallizes in a monoclinic (2/m) $P2_1/c$ space group

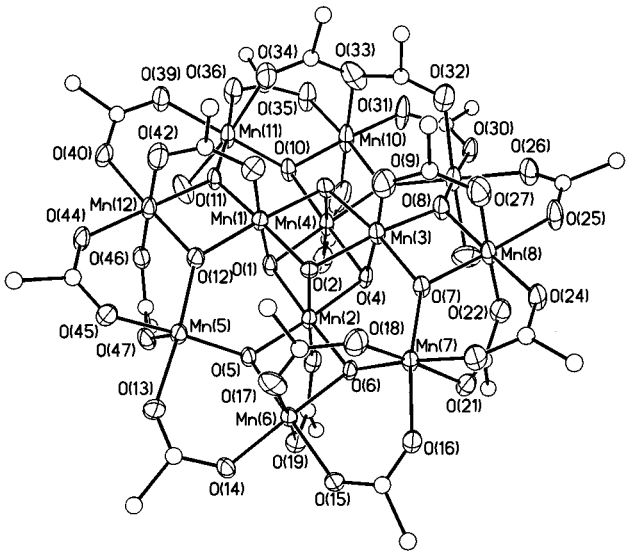

Figure 1. Plot of the anionic complex of $(PPh_4)[Mn_{12}O_{12}(O_2CPh)_{16}(H_2O)_4]\cdot 8(CH_2Cl_2)$ (**2**). The solvate molecules and the hydrogen atoms of the anion were eliminated for clarity.

with four molecules in a unit cell with $a = 13.046$ Å, $\beta = 28.223$ Å, $c = 27.162$ Å, $\beta = 96.32°$ and volume = 9940.5 Å^3. The *z*-axes of each molecule are canted relative to each other by 58.3°. Therefore, in an applied field the microcrystals orient such that the angle between the magnetic *z*-axis of each molecule and the external field axis is one-half of 58.3° or 29.15°.

The quasi-crystal HFEPR spectra collected for complex **1** at a frequency of 328.2 GHz and temperatures of 10 and 29.9 K are plotted in Figure 3. For clarity, the spectrum collected at 29.9 K is also plotted in Figure 4 where it can be seen that the peaks occur at constant spacing in magnetic field. The peaks observed correspond to transitions from M_s to $M_s + 1$ levels where, for example, the peak at 3.92 T is due to a transition from the $M_s = -19/2$ level to the $M_s = -17/2$ level. The next peak at 4.82 T is due to a transition from the $-17/2$ to the $-15/2$ level and so on, with the last observed peak at 11.7 T due to the transition from the $-1/2$ to the 1/2 level. As the temperature is increased and a greater number of M_s sublevels of the $S = 19/2$ ground state become populated, more peaks are seen at *higher* fields. Because the peaks grow in at higher fields, the sign of the zero-field splitting parameter *D* is *negative*.

Table 4. Bond Valence Sums for Each Mn Atom in Complex **2**[a]

atom	Mn^{II}	Mn^{III}	Mn^{IV}
Mn(1)	4.299 599	3.964 739	*3.890 435*
Mn(2)	4.138 817	3.816 48	*3.744 954*
Mn(3)	4.320 971	3.984 447	*3.909 773*
Mn(4)	4.486 834	4.137 392	*4.059 853*
Mn(5)	3.588 343	*3.308 878*	*3.246 865*
Mn(6)	3.694 265	*3.406 55*	3.342 707
Mn(7)	3.509 377	*3.236 061*	3.175 413
Mn(8)	3.267 247	*3.012 789*	2.956 325
Mn(9)	3.680 219	*3.393 598*	3.329 998
Mn(10)	3.573 715	*3.295 388*	3.233 628
Mn(11)	3.541 477	*3.265 661*	3.204 459
Mn(12)	3.588 622	*3.309 135*	3.247 118

[a] The calculation of a bond valence sum *s* was carried out for each Mn atom, assuming that a Mn atom is either Mn^{II}, Mn^{III}, or Mn^{IV}.

In the 10 K spectrum, the lower field peaks (3.81 and 5.75 T) and perhaps the other peaks show splittings. This could be caused by molecules having slightly different *D* values as a result of defects in the molecules or the presence of two (or more) isomeric forms of complex **1** that differ in arrangement of H_2O and carboxylate ligands. The occurrence of different isomeric forms of a given Mn_{12} complex has already been noted.[7,60] A spectrum collected at 437.69 GHz and 10 K is plotted in Figure 5. As expected, the transitions have shifted to higher fields compared with the 328.2-GHz spectrum at 10 K (Figure 3).

The resonance fields for complex **1** at all measured temperatures and frequencies are presented in Table 5. In the upper panel of Figure 6 the resonance field values are plotted versus $(2M_s + 1)$ for all the data collected. The data are divided into two groups because two different microwave frequencies were used. The lines result from a least-squares fitting of the resonance fields to eq 4, where $B_4^{0'}$ was fixed at zero. The best fit occurred for the following parameters: $S = 19/2$, $g = 1.96$,

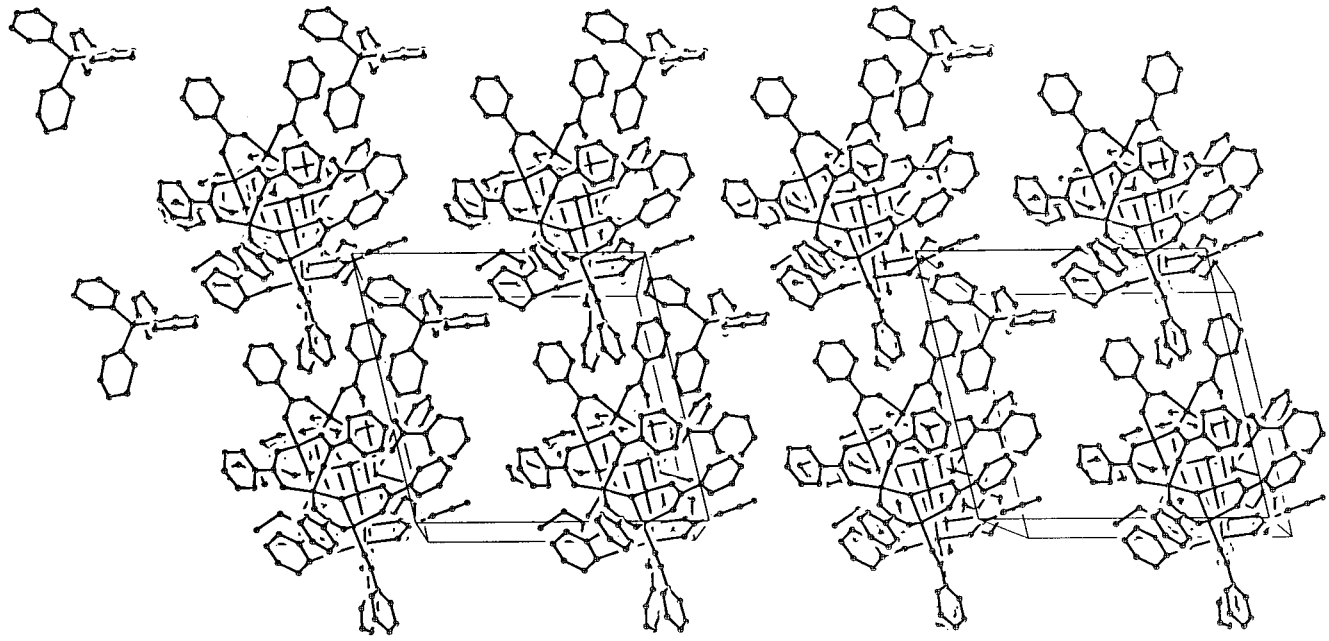

Figure 2. Stereoview of molecular packing in a unit cell for $(PPh_4)[Mn_{12}O_{12}(O_2CPh)_{16}(H_2O)_4]\cdot 8(CH_2Cl_2)$ (**2**). Solvate molecules and hydrogen atoms were eliminated for clarity.

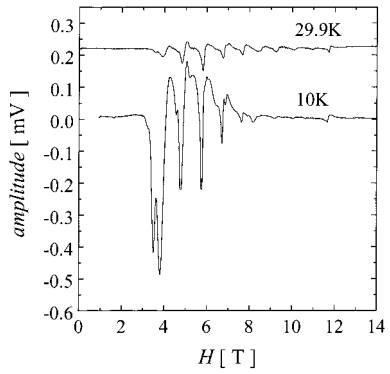

Figure 3. Pseudo−single-crystal HFEPR spectra for $(PPh_4)[Mn_{12}O_{12}(O_2CEt)_{16}(H_2O)_4]$ (**1**) collected at 328.2 GHz for temperatures 10 and 29.9 K.

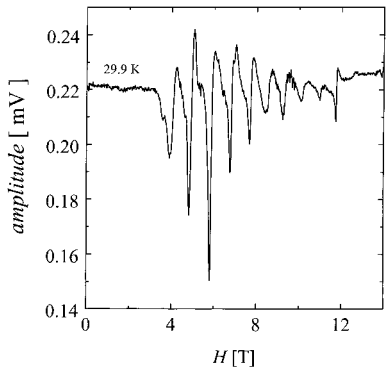

Figure 4. Pseudo−single-crystal HFEPR spectra for $(PPh_4)[Mn_{12}O_{12}(O_2CEt)_{16}(H_2O)_4]$ (**1**) collected at 328.2 GHz for temperature 29.9 K.

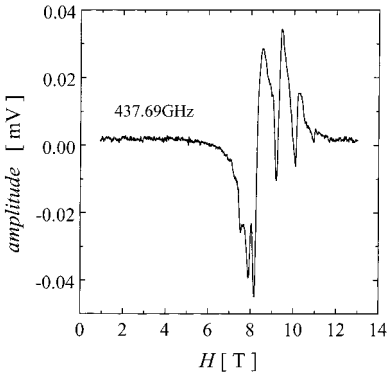

Figure 5. Pseudo−single-crystal HFEPR spectra for complex **1** collected at 437.69 GHz and 10 K.

and $D' = -0.43$ cm^{-1}. Because the angle between the magnetic *z*-axis of each molecule and the external field is 29.1°, a value of $D = -0.62$ cm^{-1} can be calculated. Inclusion of the B_4^0 term does not lead to much improvement in the least-squares fit, as seen in the lower panel of Figure 6. The fitting parameters obtained with $B_4^{0'}$ as a parameter are $S = 19/2$, $g = 1.97$, $D' = -0.42$ cm^{-1}, and $B_4^{0'} = -3.3 \times 10^{-6}$ cm^{-1}. Consideration of the angle (29.1°) between each *z*-axis of the molecule and the external field gives $D = -0.61$ cm^{-1} and $B_4^0 = -4.8 \times 10^{-6}$ cm^{-1}. The characterization of the ground state of complex **1** ($S = 19/2$, $g = 2$, and $D = -0.4$ cm^{-1}) obtained by fitting magnetization vs field data is in good agreement with HFEPR results.[5]

Alternating Current Magnetic Susceptibility Studies at Zero dc Field. The observation of a frequency-dependent out-of-phase ac magnetic susceptibility signal at zero dc field is an indicator that a molecule functions as a SMM. In the ac susceptibility experiment, the ac magnetic field is oscillated at a particular frequency. An out-of-phase ac susceptibility signal is observed when the rate at which the magnetic moment of a molecule flips is close to the operating frequency of the ac magnetic field. Thus, if a collection of SMMs are kept at a certain temperature and the frequency of the ac magnetic field is varied, a maximum in the out-of-phase ac signal will occur when the frequency of the field equals the rate at which a molecule can interconvert between the halves of the potential-energy double well shown in Figure 7. This figure shows a plot of the potential energy of one $S = 19/2$ molecule as the direction of its magnetization (magnetic moment) changes from spin "up" to spin "down". The potential energy barrier *U* is given by $U = |D|S^2$ for integer-spin complexes. Frequency-dependent out-of-phase ac susceptibility signals have been reported for all the known Mn_{12} SMMs.[4−23,28]

Ac magnetic susceptibility data not only can be used to determine whether a molecule functions as a SMM, but also to

Table 5. Pseudo−Single-Crystal HFEPR Data for $(PPh_4)[Mn_{12}O_{12}(O_2CEt)_{16}(H_2O)_4]$ (**1**)

	transition field, *H* (T)		
transitions $M_s \Rightarrow M_s + 1$	328.2 GHz, 29.9 K	328.2 GHz, 10 K	437.69 GHz, 10 K
			7.52 (sh)[a,b]
	3.58 (w)[a,c]	3.494[a]	7.901[a]
−19/2 → −17/2	3.92	3.807	8.17
−17/2 → −15/2	4.825	4.772	9.197
−15/2 → −13/2	5.807	5.75	10.089
−13/2 → −11/2	6.761	6.715	10.94
−11/2 → −9/2	7.676	7.621 (w)	
−9/2 → −7/2	8.41 (w)	8.178 (w)	
−7/2 → −5/2	9.225 (w)	9.165 (vw)	
−5/2 → −3/2	10.1 (w)		
−3/2 → −1/2	10.97 (w)		
−1/2 → 1/2	11.75[a]		

[a] Doubling of peaks. [b] (sh) = shoulder. [c] (w) = weak intensity peak. [d] (vw) = very weak intensity peak. [e] Peak enhanced because of impurity.

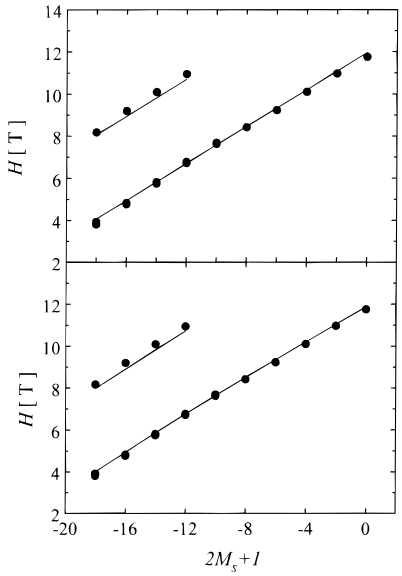

Figure 6. Plot of resonance field vs $2M_s + 1$ taken from the pseudo−single-crystal HFEPR data collected on complex **1** at frequencies 328.2 and 437.69 GHz for temperatures 10 and 29.9 K (●). At the top of the figure the solid line is a least-squares fitting of these data to eq 4 with $\theta = 29.1°$, and $B_4^{0'}$ is held fixed at zero. At the bottom of the figure the solid line is again a least-squares fitting of the data to eq 4 where $\theta = 29.1°$, but this time $B_4^{0'}$ is *not* fixed.

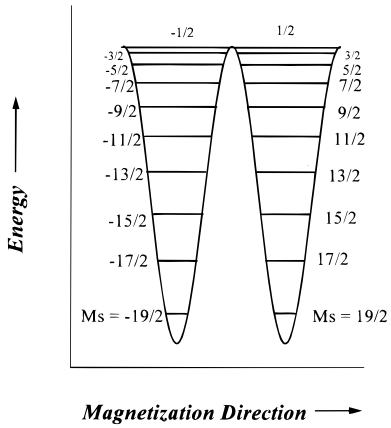

Figure 7. Plot of potential energy vs the magnetization direction for a single molecule with a $S = 19/2$ ground state split by axial zero-field splitting. The potential energy barrier height is therefore $90|D|$ for the thermally activated process involving converting the magnetic moment of the molecule from the "spin up" $M_s = 19/2$ level to the "spin down" $M_s = -19/2$ level.

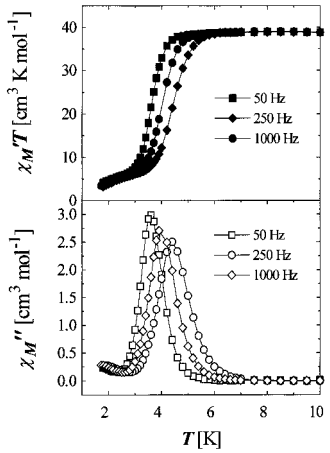

Figure 8. Plots of $\chi'_M T$ vs T (top) and χ''_M vs T (bottom) for complex $(PPh_4)[Mn_{12}O_{12}(O_2CPh)_{16}(H_2O)_4]$ (**2**) in a 1.0 Oe ac field oscillating at the indicated frequencies (with no applied dc field), where χ'_M and χ''_M are the in-phase and the out-of-phase magnetic susceptibility, respectively.

obtain the effective energy barrier (U_{eff}) for magnetization relaxation and the spin of the ground state. Ac magnetic susceptibility data were collected for complex **2**. A polycrystalline sample of complex **2** was studied in the 1.7−30 K range with a 1.0 Oe ac field oscillating at various frequencies as indicated in Figure 8. The external dc magnetic field was held at zero. The upper panel shows a plot of the product of in-phase component of the ac susceptibility and the temperature $\chi_M'T$ vs the temperature, and the lower panel is a plot of the out-of-phase susceptibility χ_M'' vs temperature. Frequency-dependent out-of-phase ac signals are seen for complex **2**, which indicates that complex **2** functions as a SMM. One peak is observed in the range of 3−6 K for complex **2** in the frequency range of 1−1512 Hz. There is only one magnetization relaxation process seen for complex **2**. The value of $\chi_M'T$ at its low-temperature plateau in Figure 8 can be used to determine the ground state for complex **2**. If it is assumed that only the ground state of complex **2** is thermally populated in the 5−10 K range, then the value of $\chi_M'T$ indicates a $S = 19/2$ ground state with $g = 1.8$.

Magnetization relaxation times (τ) are obtained from the relationship $\omega\tau = 1$ at the maxima of the χ_M'' vs temperature curves.[20] The χ_M'' peak positions were determined by fitting

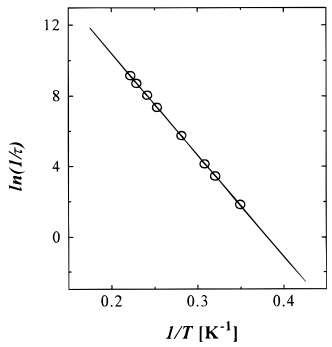

Figure 9. Plot of relaxation rate vs reciprocal temperature for complex **2** in zero dc field in the range from 0.1 to 1512 Hz of oscillating frequencies. The data partially shown in Figure 8 were analyzed to give this plot of $\ln(1/\tau)$ vs $1/T$ and the solid line is least-squares fitted to Arrhenius eq 5.

Table 6. Temperature Corresponding to the Maximum in χ''_M at Various Frequencies and the Magnetization Relaxation Rates ($1/\tau$) at Zero dc Field for Complex **2**

temp (K)	frequency (Hz)	relaxation rate (s^{-1})	relaxation time (s)
2.862 9	1	6.283 18	0.159 155
3.121 7	5	31.415 9	0.031 831
3.244 7	10	62.831 8	0.015 916
3.558 9	50	314.159	0.003 183
3.96	250	1 570.795	0.000 637
4.147 3	499	3 135.307	0.000 319
4.371 5	977	6 138.667	0.000 163
4.509 8	1510	9 487.610	0.000 105

the χ_M'' vs temperature data to a Lorentzian function. A plot of $\ln(1/\tau)$ vs $1/T$ is given in Figure 9 for complex **2**; the data used for this Arrhenius plot are listed in Table 6. The magnetization relaxation rate ($1/\tau$) follows the Arrhenius equation. This is the characteristic behavior for a thermally activated Orbach process. The theoretical equation for this process is given as:

$$\frac{1}{\tau} = \frac{1}{\tau_o}\exp(-U_{eff}/kT) \qquad (5)$$

where U_{eff} is the effective anisotropy energy barrier, k is the Boltzmann constant, and T is the temperature. The solid line in Figure 9 shows the result of a least-squares fit of the ac susceptibility relaxation data to eq 5. For complex **2**, the effective energy barrier is 57.5 K with an attempt frequency of $1/\tau_0 = 3.1 \times 10^{-10}$ s. This barrier is lower than the value (62 K) obtained by fitting the ac susceptibility data for $Mn_{12}Ac$ (**1**).[12] The effective barrier (U_{eff}) for complex **2** is in good agreement with the thermodynamic energy barrier calculated as $U = |D|S^2 = 56$ K for $S = 19/2$ and $D = -0.44$ cm^{-1}.

More detailed ac magnetic susceptibility experiments were carried out on complex **1** than on complex **2**. Magnetization relaxation data were collected while holding the temperature of the microcrystalline sample of complex **1** constant and varying the frequency of the ac magnetic field in dc field. The magnetization relaxation was probed in the temperature range of 3.2 to 7.2 K. At a fixed temperature, the in-phase (χ'_M) and the out-of-phase (χ''_M) components of the ac magnetic susceptibility were measured as the frequency (ω) of the ac field (0.05 Oe amplitude) was varied from 0.01 to 1500 Hz. These data were best fit to a distribution of single relaxation processes rather than a single relaxation process. For a single relaxation process, $\chi'_M(\omega)$ and $\chi''_M(\omega)$ are given by eqs 6 and 7, respectively.

$$\chi'(\omega) = \chi_S + \frac{(\chi_T - \chi_S)}{1 + \omega^2\tau^2} \quad (6)$$

$$\chi''(\omega) = \frac{(\chi_T - \chi_S)\omega\tau}{1 + \omega^2\tau^2} \quad (7)$$

In these equations, $\chi_s = \chi_{w\Rightarrow\infty}$ is the adiabatic susceptibility, $\chi_T = \chi_{\omega\Rightarrow\infty}$ is the isothermal susceptibility, $\omega = 2\pi\nu$ is the angular frequency, and τ is the magnetization relaxation time. The isothermal susceptibility, χ_T, is the dc susceptibility for paramagnets observing the Curie law. For a distribution of single relaxation processes, the expressions for $\chi'(\omega)$ and $\chi''(\omega)$ are given as:[74h]

$$\chi'(\omega) = \chi_S + \frac{(\chi_T - \chi_S)[1 + (\omega\tau)^{1-\alpha}\sin {}^1/_2\alpha\pi]}{1 + 2(\omega\tau)^{1-\alpha}\sin {}^1/_2\alpha\pi + (\omega\tau)^{2(1-\alpha)}} \quad (8)$$

$$\chi''(\omega) = \frac{(\chi_T - \chi_S)(\omega\tau)^{1-\alpha}\cos {}^1/_2\alpha\pi}{1 + 2(\omega\tau)^{1-\alpha}\sin {}^1/_2\alpha\pi + (\omega\tau)^{2(1-\alpha)}} \quad (9)$$

where α is a value between 0 and 1 and gauges the width of the distribution. When $\alpha = 0$, eqs, 8 and 9 reduce to eqs 6 and 7, respectively, describing a single relaxation process. A distribution of single relaxation processes as given in eqs 8 and 9 has been used extensively in describing ac magnetic susceptibility data [both $\chi'_M(\omega)$ and $\chi''(\omega)$] for glasses,[74b−d,74h] as well as for dielectric relaxation in molecules.[74c]

In Figure 10 are shown plots of χ'_M vs frequency and χ''_M vs frequency for a microcrystalline sample of complex **1** at 4.2 K. The dashed lines result from least-squares fitting of the data to a single relaxation process, as described by eqs 6 and 7 to give $\chi_s = 2.47$ cm^3 mol^{-1}, $\chi_T = 11.3$ cm^3 mol^{-1}, and $\tau = 0.00769$ s. Considerably improved fits are obtained when the data are fit to a distribution of single relaxation processes, as described in eqs 8 and 9. This gives the parameters of $\chi_S = 1.68$ cm^{3}mol^{-1}, $\chi_T = 12.16$ cm^3 mol^{-1}, $\tau = 0.00801$ s, and $\alpha = 0.260$. The resulting relaxation times (τ) obtained at a given temperature from these two fitting schemes are very similar. The main difference in fitting parameters occurs in the values of χ_T and χ_S. In Figure 11 is given a plot of χ''_M vs χ'_M at 4.2 K, otherwise known as a Cole−Cole plot or an Argand plot. This type of plot is used to decide whether one or more relaxation processes are present. If it is symmetric, then it is likely that only one process is present. Such is the case for complex **1**. Again it is clear that fitting the data to a distribution of single relaxation processes (solid line) results in a better fit than fitting the data to a single relaxation process (dashed line). From these data it can be concluded that there is only one magnetization relaxation process present for complex **1**. Moreover, there is a distribution in this single relaxation process. This could result from a situation in which there are molecules in the microcrystalline sample exhibiting a distribution in effective energy barriers, i.e., a narrow range in U_{eff} values. It is likely there is a distribution in environments of Mn_{12} molecules in the crystals resulting from the presence of defects in the crystals. Such a distribution in Mn_{12} molecule environments would lead to a distribution of zero-field splitting parameters, D. This affects the potential-energy barrier height. A distribution in transverse zero-field interactions could also affect the rate of magnetization quantum tunneling.

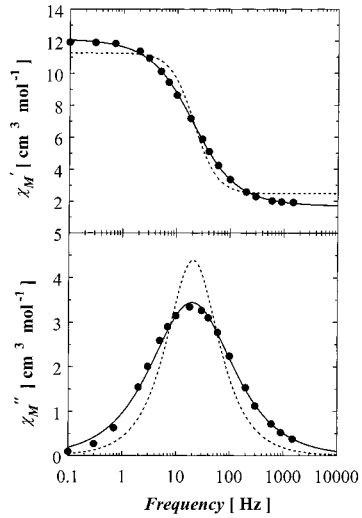

Figure 10. Plot of χ'_M versus frequency (O, top) and χ''_M versus frequency (O, bottom) at temperature 4.2 K for $(PPh_4)[Mn_{12}O_{12}(O_2CEt)_{16}(H_2O)_4]$ (**1**). The dotted lines are least-squares fitting of the data to a single relaxation process as described by eqs 6 and 7 giving $\chi_S = 2.47$ cm^3 mol^{-1}, $\chi_T = 11.3$ cm^3 mol^{-1}, and $\tau = 0.00769$ s. The solid lines are least-squares fitting of the data to a distribution of single relaxation processes as described in eqs 8 an 9 yielding parameter values, $\chi_S = 1.68$ cm^3 mol^{-1}, $\chi_T = 12.16$ cm^3 mol^{-1}, and $\tau = 0.00801$ s and $\alpha = 0.260$.

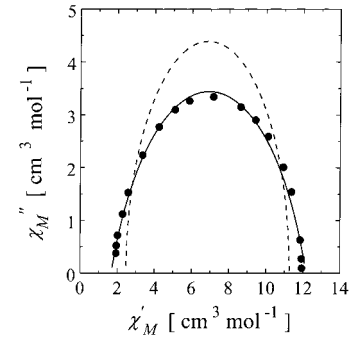

Figure 11. Plot of χ''_M vs χ'_M at 4.2 K otherwise known as a Cole−Cole plot or an Argand plot for $(PPh_4)[Mn_{12}O_{12}(O_2CEt)_{16}(H_2O)_4]$ (**1**). The solid line is a least-squares fitting of the data (O) to a distribution of single relaxation processes (eq 8) whereas the dotted line is a fit of the data to a single relaxation process (eq 6).

Similar results were obtained at temperatures other than 4.2 K. In Figure 12 χ'_M vs frequency (upper panel) and χ''_M vs frequency (lower panel) are plotted for a microcrystalline sample of complex **1** at temperatures of 3.2, 3.8, and 5.4 K. The data fit well to a distribution of single relaxation processes (eqs 8 and 9) as indicated by the solid lines in Figure 12. The fit to a single relaxation process is poor. The fitting parameters obtained by fitting $\chi'_M(\omega)$ to eq 8 in the temperature range of 3.2 to 7.2 K are listed in Table 7. The magnetization relaxation data collected for complex **1** will be analyzed to check for compliance to an Arrhenius-type response. However, before this is discussed, we will first describe how additional relaxation data were obtained for complex **1** below 3.2 K.

(74) (a) van Duyneveldt, A. J. In *Magnetic Molecular Materials*; Gatteschi, D.; Kahn, O.; Miller, J.; Palacio, F.; Eds.; Kluwer Academic Publishers: London, 1991; P 353. (b) Chamberlin, R. V.; Mozurkewich, G.; Orbach, R. *Phys. Rev. Lett*. **1984**, *52*, 867. (c) De Dominicis, C.; Orland, H.; Lainée, F. *J. Phys. Lett*. **1985**, *46*, L-463. (d) Weiss, G. H.; Dishon, M.; Long, A. M.; Bendler, J. T.; Jones, A. A.; Inglefield, P. T.; Bandis, A. *Polymer* **1994**, *35*, 1880. (e) Cumbrera, F. L.; Sanchez-Bajo, F.; Guiberteau, F.; Solier, J. D. *J. Mater. Sci*. **1993**, *28*, 5387. (f) Hoffman, J. D.; Pfeiffer, H. G. *J. Chem. Phys*. **1954**, *22*, 132. (g) Chung, S. H.; Stevens, J. R. *Am. J. Phys*. **1991**, *59*, 1024. (h) Cole, K. S.; Cole, R. H. *J. Chem. Phys*. **1941**, *9*, 341.

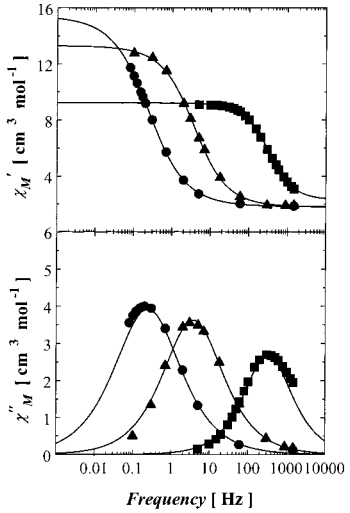

Figure 12. Plot of χ'_M vs frequency (top) and χ''_M vs frequency (bottom) at temperatures 3.2 (○), 3.8 (△), and 5.4 K (□) for $(PPh_4)[Mn_{12}O_{12}(O_2CEt)_{16}(H_2O)_4]$ (**1**). The solid lines are least-squares fitting of the data to a distribution of single relaxation processes as described in eqs 8 and 9.

Table 7. Relaxation Fitting Parameters from Least-Squares Fitting of $\chi'_M(\omega)$ Data for a Microcrystalline Sample of Complex **1** to a Distribution of a Single Relaxation Process (Eq 8)

T (K)	τ (s)	χ_S (cm^3 mol^{-1})	χ_T (cm^3 mol^{-1})	α
3.2	0.657	1.80	15.4	0.334
3.4	0.268	1.79	15.2	0.327
3.6	0.103	1.81	14.2	0.309
3.8	0.0427	1.76	13.3	0.286
4.2	0.00801	1.68	12.1	0.26
4	0.0170	1.82	12.8	0.245
4.6	0.00372	1.66	11.1	0.258
4.8	0.00206	1.71	10.5	0.238
5	0.00122	1.76	10.1	0.228
5.2	7.39E−04	1.95	9.63	0.197
5.4	4.85E−04	2.26	9.21	0.162
5.6	3.34E−04	2.26	8.86	0.13
5.8	2.42E−04	3.10	8.54	0.0985
6	1.82E−04	3.66	8.25	0.0699
6.2	1.38E−04	4.13	7.99	0.053
6.4	1.05E−04	4.58	7.75	0.0377
6.6	6.60E−05	4.39	7.53	0.0165
6.8	6.41E−05	5.46	7.39	0[a]
7	4.78E−05	5.84	7.19	0[a]
7.2	2.48E−05	5.9	7.00	0[a]

[a] These parameter values were fixed at zero.

Magnetization Decay in Zero dc Field for Complex 1. To characterize the slow magnetization relaxation at even lower temperatures for $(PPh_4)[Mn_{12}O_{12}(O_2CEt)_{16}(H_2O)_4]$ (**1**), magnetization decay experiments were carried out in zero dc field in the temperature range of 1.8−2.5 K. The microcrystalline sample of $(PPh_4)[Mn_{12}O_{12}(O_2CEt)_{16}(H_2O)_4]$ (**1**) was restrained in Parafilm, and the decay in magnetization was measured as a function of time using a MPMS-EXEL SQUID magnetometer. The temperature was reduced to the desired temperature, and the magnetic moment of the sample was saturated in a field of 30 kOe. The magnet was then quenched, followed by the measurement of magnetization decay as a function of time in zero field. Data were collected for up to 40 h. A plot of the natural logarithm of magnetization versus time for $(PPh_4)[Mn_{12}O_{12}(O_2CEt)_{16}(H_2O)_4]$ (**1**) at temperatures 1.8, 2.0, 2.1, 2.4, and 2.5 K is shown in Figure 13.

Initial efforts showed that the decay data collected at each temperature could not be well fit by a single-exponential decay curve. These data are best fit to a distribution of a single-exponential decay as plotted in Figure 13. The distribution of a single-exponential decay or "stretched" exponential decay is given as

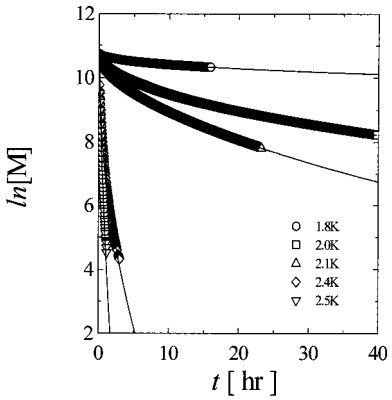

Figure 13. Natural logarithm of magnetization vs time collected on a microcrystalline sample of $(PPh_4)[Mn_{12}O_{12}(O_2CEt)_{16}(H_2O)_4]$ (**1**) at temperatures 1.8 (○), 2.0 (□), 2.1 (△), 2.4 (◇), and 2.5 (▽) K. Saturation of the moment was first achieved at the desired temperature in a field of 30 kOe, followed by quenching the field and measuring. The line is a least-squares fitting of the data to a stretched single-exponential decay (eq 10).

$$M = M_o \exp[-(t/\tau)^B] \quad \text{or} \quad \ln(M) = \ln(M_o) - (t/\tau)^B \tag{10}$$

This equation describes a decay that is initially fast and then becomes slower with time. M_o is the initial magnetization, τ is the average relaxation time, and B is the width of the distribution. When $B = 1$ the relaxation as a function of time follows a single-exponential decay. A distribution of a single relaxation process as described in eq 10 has been widely used in modeling the magnetization decay data of spin glasses[74a−c] and polymers,[74d] mechanical stress relaxation in CoO for example,[74e] and dielectric relaxation.[74e−g] Most recently eq 10 also has been used in describing the magnetization relaxation decay in the single molecule magnet $[Fe_8O_2(OH)_{12}(tacn)_6]^{8+}$, where tacn is triazacyclononane.[16]

Attempts to fit the data to a single-exponential process (eq 10 when $B = 1$) lead to poor fits. Fitting to a single exponential was possible only if the tail of the magnetization decay was fit ignoring the initial magnetization decay. At low temperatures this required discarding >30% of the data. For example, at 2.0 K only the magnetization decay beyond 15 h was fit, whereas at 2.1 K only data beyond 12 h were considered. A single exponential decay clearly is not sufficient in describing the magnetization decay in its entirety. The relaxation times obtained using the two different fitting schemes are summarized in Table 8.

Magnetization relaxation data have been collected for complex **1** in the 3.2−7.2 K range with the ac susceptibility technique and in the 1.8−2.5 K range via dc field magnetization decay experiments. All these data are plotted together in Figure 14, which gives an Arrhenius plot of the natural logarithm of the relaxation rate $^1/_\tau$ vs $1/T$. Least-squares fitting of all data to the Arrhenius equation gives a good fit (solid line in Figure 14) with the parameters $U_{eff} = 57$ K and $\tau_0 = 1.4 \times 10^{-8}$ s (or $^1/_{\tau_0} = 7.2 \times 10^7$ s^{-1}). This value of U_{eff} can be compared with the thermodynamic potential-energy barrier (Figure 7) for a single $S = 19/2$ molecule to be thermally activated over the barrier. From the HFEPR experiments and previous dc magnetization data[5] the ground-state spin of complex **1** was

Table 8. Relaxation Fitting Parameters τ, ln(M_o), and B Resulting from Least-Squares Fitting of Magnetization Decay Data for a Microcrystalline Sample of Complex 1[a]

	stretched exponential decay (eq 10)			single-exponential decay (eq 10 where $B = 1$)	
temp (K)	τ (hr)	ln(M_o)	B	τ (hr)	ln(M_o)
1.8	101	10.8	0.396	46.9	10.6
2	5.95	10.8	0.494	25.8	9.73
2.1	3.55	10.7	0.570	11.6	9.77
2.4	0.0650	10.7[b]	0.493	0.613	8.58
2.5	0.0686	10.7[b]	0.724	0.180	9.94

[a] The data were least-squares fit to a stretched-exponential decay (eq 4) and to a single-exponential decay (eq 4, where $B = 1$). [b] Held constant.

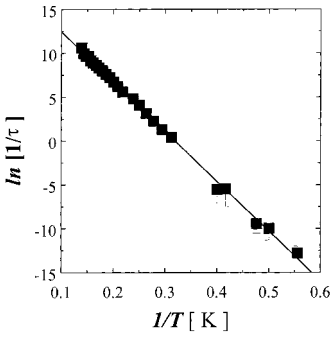

Figure 14. Plot of natural logarithm of rate ($1/\tau$) vs inverse of temperature ($1/T$) for $(PPh_4)[Mn_{12}O_{12}(O_2CEt)_{16}(H_2O)_4]$ (**1**) in the temperature range of 1.8−7.4 K. The line is a least-squares fit to the Arrhenius equation, describing a thermally activated process where $U = 57$ K and $\tau_o = 1.4 \times 10^{-8}$ s.

determined to be $S = 19/2$ with $D = -0.62$ cm^{-1}. This gives a barrier of $(D\hat{S}_z^2) = [(^{19}/_2)^2 - (^1/_2)^2] \times |D| = 79$ K. Clearly, the value of U_{eff} is less than the barrier height U, which likely results from the presence of magnetization quantum mechanical tunneling. In other words, not all the complexes are thermally activated over the barrier shown in Figure 7. Instead, many complexes tunnel through the barrier between, for example, the $M_s = -^5/_2$ and $M_s = +^5/_2$ levels. Quantum magnetization tunneling leads to a kinetic barrier (U_{eff}) that is smaller than the thermodynamic barrier. Previously it was mentioned that magnetization quantum tunneling is forbidden in half-integer spin ground-state complexes in the *absence* of magnetic field. However, the data above strongly suggest that quantum mechanical tunneling is playing a part in magnetization relaxation. The origin of the magnetization tunneling is likely the presence in each $[Mn_{12}]^-$ molecule of a 50−100 G internal magnetic field due to the nuclear spins on the Mn atoms. Thus quantum tunneling is not forbidden.

Concluding Comments

The single-crystal X-ray structure of $(PPh_4)[Mn_{12}O_{12}(O_2CPh)_{16}(H_2O)_4]\cdot 8CH_2Cl_2$ (**2**·$8CH_2Cl_2$) was determined. Unlike the propionate analogue, it is not possible to tell whether the Mn atom valences, formally $Mn^{IV}_4Mn^{III}_7Mn^{II}$, are trapped or partially delocalized in the $[Mn_{12}]^-$ anion in complex **2**. Definitive HFEPR data were collected for $(PPh_4)[Mn_{12}O_{12}(O_2CEt)_{16}(H_2O)_4]$ (**1**) to show that the anionic complex has a $S = 19/2$ ground state, experiencing axial zero-field splitting ($D\hat{S}_z^2$) with $D = -0.62$ cm^{-1}. The $[Mn_{12}]^-$ anions in complexes **1** and **2** exhibit slow magnetization relaxation at low temperatures. Both of these anionic complexes are functioning as single-molecule magnets. This is indicated by magnetization hysteresis data presented previously as well as the detailed ac magnetic susceptibility data presented in this article. An analysis of the Cole−Cole plot of ac susceptibility data for complex **1** shows that there is only one magnetization relaxation process present. The magnetization relaxation rate data for complexes **1** and **2** fit an Arrhenius plot. The effective energy barriers for magnetization relaxation obtained by the Arrhenius fit of the rate data are smaller than the thermodynamic barriers calculated by knowing the ground-state spin S and the zero-field splitting parameter D. This reflects the presence of quantum mechanical tunneling of the direction of magnetization for each $[Mn_{12}]^-$ molecule.

Acknowledgment. This work was supported by the National Science Foundation (G.C. and D.N.H.) and the NHMFL Science Program and NHMFL User Program. The ac magnetic susceptibility measurements were performed with a MPMS2 SQUID magnetometer provided by the Center for Interface and Material Science, funded by the W. M. Keck Foundation.

Supporting Information Available: Tables listing detailed crystallographic data of atomic positional coordinates, all bond distances and angles, and anisotropic displacement parameters. This information is available free of charge via the Internet at http://pubs/acs.org.

IC990613G